Eur. Phys. J. D (2012) 66: 134
DOI: 10.1140/epjd/e2012-20657-8

THE EUROPEAN PHYSICAL JOURNAL D

Regular Article

# Slow metastable $H(2^2S_{1/2})$ from dissociation of cold $H_2$ induced by electrons

A. Medina[1,2,a], G. Rahmat[2], G. Jalbert[2,3], R. Cireasa[2,4], F. Zappa[5], C.R. de Carvalho[2,3], N.V. de Castro Faria[2,3], and J. Robert[2]

[1] Instituto de Física, Universidade Federal da Bahia, 40210-340 Salvador, BA, Brazil
[2] Laboratoire Aimé Cotton CNRS, Université Paris Sud 11, 91405 Orsay Cedex, France
[3] Instituto de Física, UFRJ, Cx. Postal 68528, 21941-972 Rio de Janeiro, RJ, Brazil
[4] Laboratoire Collisions Agrégats Réactivité, IRSAMC, Université Paul Sabatier, 31062 Toulouse Cedex 09, France
[5] Departamento de Física, UFJF, MG 36036-330 Juíz de Fora, Brazil

Received 11 November 2011 / Received in final form 13 February 2012
Published online 23 May 2012 – 

**Abstract.** We have produced slow metastable $H(2^2S_{1/2})$ coming from the dissociation of cold $H_2$ induced by electron collisions. The experiment consisted of a supersonic jet of $H_2$ crossing electrons produced by a high intensity pulsed electron gun. The neutral fragments were detected through electric field induced Lyman-$\alpha$ radiation and their velocities were measured by time-of-flight (TOF) technique. The main characteristics of our experiment are the low molecular temperature, the long flight path and the small well defined collision and electric field regions. They give rise to precise velocity measurements and, consequently, to good spectra resolution. We have performed a careful analysis of the electron-molecule collision kinematical effects in order to identify which vibrational levels can be involved in the transition. Our results also explain the origin of the TOF peak widths. Relative probabilities to produce these levels have been deduced.

## 1 Introduction

Although the $H_2$ molecule has been studied for a long time, several of their ro-vibrationals levels are not completely known yet and are the subject of recent research, see reference [1] and references therein. Regarding the applied point of view, the processes of excitation, emission and fragmentation of molecular hydrogen plays an important role in astrophysics and plasma physics. For instance, the determination of the Saturn atmospheric structure, such as the H and $H_2$ mixing ratio, also requires the knowledge of accurate excitation, emission and dissociation cross sections of $H_2$ by photons and electrons [2]. Moreover, the emission from molecular hydrogen is an important diagnostic probe of the peripheral regions of high-temperature fusion plasmas [3]. The dissociation of molecular hydrogen has also been theoretically investigated. An extensive study of the doubly excited states of $H_2$ converging to the $H(n = 2) + H(n' = 2)$ limit has been performed [4]. The calculations furnished potential energy curves for all internuclear distances. Recently, the competing decay channels of photoexcited long-lived superexcited $H_2$ molecular levels have had their absolute cross sections measured from the ionization threshold of $H_2$ up to the $H(1^2S_{1/2})+H(n = 3)$ dissociation limit [5]. The inverse process, the formation of $H_2$ from collisions of two $H(2^2S_{1/2})$ atoms, has been object of study, both theoretically, for atoms at thermal temperatures [6] and experimentally, at low temperatures [7].

In the 60s, Leventhal et al. [8] observed the time-of-flight (TOF) distribution of $H(2^2S_{1/2})$ atoms produced by $H_2$ dissociation and showed the existence of two groups, one with energies centred at about 5 eV and other with energies centred at about 0.3 eV; these two distinct groups of metastable atoms have been called fast and slow fragments. In Figure 1 we can recognize the origin of each group. These atoms have been studied from this pioneer article of 1967 [8] to recent years. The slow $H(2^2S_{1/2})$ atoms, in which we are interested in the present work, are formed by the dissociation of $H_2$ molecules excited into bound vibrational levels of singly excited electronic states. The singly excited states can dissociate in $H(1s) + H(nl)$ while the doubly excited states can lead to fast metastable twin hydrogen atoms. The fast $H(2^2S_{1/2})$ atoms have been investigated in our previous work [9].

In this article we report the measurement of slow $H(2^2S_{1/2})$ atoms coming from the dissociation of cold $H_2$ molecules once excited by electron collisions. The experiment is described in Section 2. A theoretical analysis of the kinematical effects is carried out in Section 3, with the use of relevant Newton diagrams for the two processes involved: (i) electronic excitation and associated molecular recoil, (ii) dissociation of the excited molecule. In Section 4

[a] e-mail: aline.medina@ufba.br

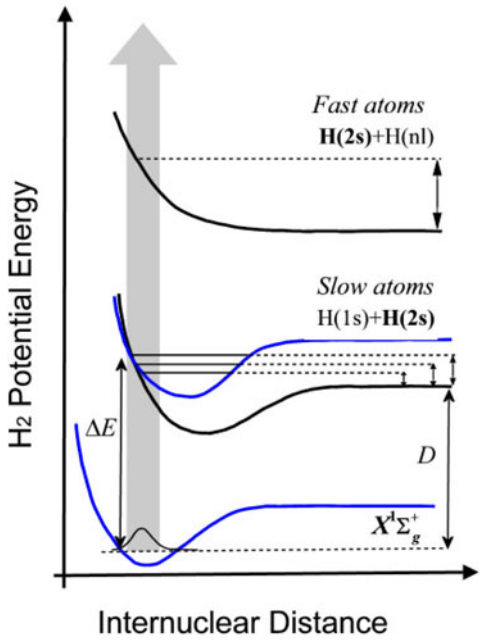


**Fig. 1.** (Color online) Rough schema of the potential energy curves of the $H_2$ molecule, as a function of the internuclear distance, illustrating the origin of $H(2^2S_{1/2})$ atoms. The fast atoms are originated in repulsive doubly excited states while the slow ones originates from bound singly excited states.

we present and compare the experimental and the simulated time-of-flight spectra to ascertain the origin, with respect to the molecular frame, and the width of each peak. We left our conclusions to Section 5.

## 2 Experiment

By using the experimental set-up schematically presented in Figure 2 and already described in reference [9], we have measured time-of-flight distributions of $H(2^2S_{1/2})$ metastable atoms produced by dissociation of $H_2$ molecules through electron impact. The $H_2$ molecular jet and the electron beam intersect each other at a right angle. The molecular hydrogen beam is produced by a continuum (CW) Campargue-type supersonic nozzle source [10], which allows a relative velocity spread of the order of 0.01, well defined initial molecular states and high target density. The measured mean velocity of the hydrogen molecules in the supersonic jet is 2.7 km/s [11]. The jet has rotational temperature of about 1 K and vibrational temperature of about 10 K. Because of the expansion, essentially all hydrogen molecules are on the ro-vibrational levels $v = 0$, with $J = 0$ or $J = 1$ [12]. In the collision region the $H_2$ beam has approximately 3 mm of diameter and the flow is $10^{22}$ molecules per steradian per second, which corresponds to $(2.3 \pm 0.2) \times 10^3$ molecules per microsecond per cubic millimeter at the collision volume. The vacuum in the collision chamber was maintained in the range $5\times10^{-7}$ to $1.2\times10^{-6}$ torr by a 2000 L/s diffusion pump.

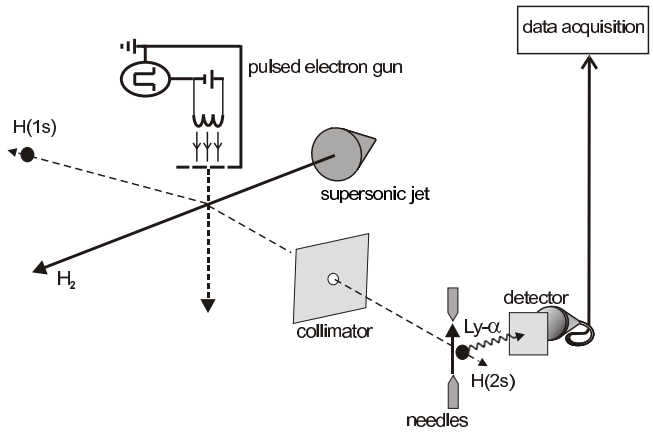


**Fig. 2.** Schematic view of the experimental set-up.

The electron beam was pulsed and the pulse duration could be chosen in the range of 0.2 to 2 $\mu$s. The electron energy is given by the difference between the potential of the filament and that of the interaction region, which has to be grounded in order to avoid the disappearance of $H(2^2S_{1/2})$ atoms through the coupling with radiative $H(2^2P_{1/2})$ states.

Different from our earlier work, in the present experiment we have used only one detection system, that was placed at 230 mm from the collision region. This distance precludes the arrival of excited $H(2^2P_{1/2})$ atoms since, because of their lifetime of few nanoseconds, they decay after traveling only a few millimeters, even in the case of the fastest fragments. The detection of the $H(2^2S_{1/2})$ atoms occurs by quenching the $2^2S_{1/2}$ and the $2^2P_{1/2}$ states of the atoms, so that they can decay to the $1^2S_{1/2}$ state emitting a Lyman-$\alpha$ radiation (1216 Å) which is detected by a channel electron multiplier.

The beginning of the electron pulse sets the start of our time-of-flight measurement. Pulses from the detector are separately pre-amplified and amplified by standard NIM electronics. After discrimination from electronic noise, the signals are fed as stop pulses of a "FAST ComTec" time analyser card.

## 3 Collision kinematics

In order to identify the molecular vibrational levels of the singly excited states related to the slow $H(2^2S_{1/2})$ peaks present in our experimental spectra, we present a theoretical study of the inelastic collision between an electron and a $H_2$ molecule followed by its subsequent dissociation. In addition, we determine the relative importance of the kinematical parameters on the peak resolution as a function of the fragments time-of-flight. The calculations are performed in two steps: first we analyse the electron-molecule collision, in their plane, and the possible recoil angles of the excited $H_2$ molecule; second, we considere the molecular dissociation and the possible fragmentation angles of the neutral atoms pair. Even if the fragmentation is assumed to be isotropic in the molecular frame (CM), this

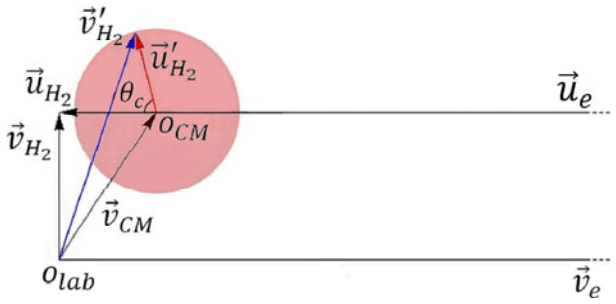


**Fig. 3.** (Color online) The Newton diagram representing the electron-molecule collision. The origins of the coordinate systems are represented by $O_{lab}$ and $O_{CM}$. $\boldsymbol{v}_{CM}$ is the system centre of mass velocity vector, $\boldsymbol{v}_{H_2}$ and $\boldsymbol{v}_{e^-}$ are the initial lab velocity vectors, $\boldsymbol{u}_{H_2}$ and $\boldsymbol{u}_{e^-}$ are the initial CM velocity vectors. The final molecular velocity vectors are, in the lab, $\boldsymbol{v}'_{H_2}$, and in the CM, $\boldsymbol{u}'_{H_2}$. The later is defined by an azimuthal angle $\phi_c$ (not shown), referenced to $\boldsymbol{u}_{H_2}$, and $\theta_c$. As the electron energy is 120 eV, which represents an electron velocity much bigger than all other constraints, its lab and CM velocity vectors could not be entirely shown in the figure.

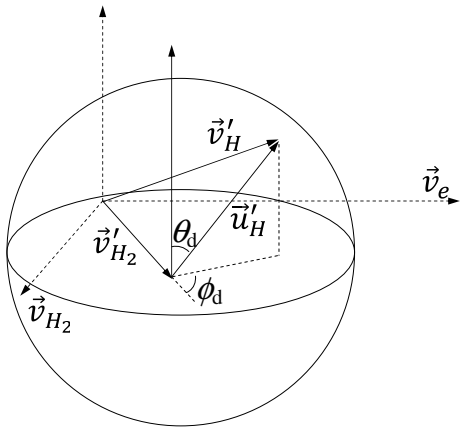


**Fig. 4.** Three dimensional Newton diagram representing the $H_2$ dissociation. $\boldsymbol{v}'_{H_2}$ is the centre of mass velocity of the two atoms system, $u'_H$ is the CM final velocity of the $H(2^2S_{1/2})$ atom, and $v'_H$ is this velocity in the laboratory frame. The molecule and the electron initial velocities are also shown. For better visualization the graph is not at scale.

property does not remain in the laboratory frame (lab) where the experiment is performed. Thus, one important aspect to be considered is the transformation of CM to lab variables, both systems expressed here in spherical coordinates. By the Newton diagrams we can compute final velocity vectors as a function of initial velocity vectors using energy and momentum conservation.

In the first step, involving the electron-molecule collision, the CM system moves with the velocity and direction of the electron-molecule centre of mass velocity:

$$\boldsymbol{v}_{CM} = \frac{m_{H_2}}{m_{H_2} + m_{e^-}}\boldsymbol{v}_{H_2} + \frac{m_{e^-}}{m_{H_2} + m_{e^-}}\boldsymbol{v}_{e^-}. \quad (1)$$

with $m_{H_2}$ and $m_{e^-}$ representing the molecule and the electron mass, respectively, and $\boldsymbol{v}_{H_2}$ and $\boldsymbol{v}_{e^-}$ their known lab velocities. The initial and final velocities transform from CM to lab frame as follows

$$\begin{aligned} \boldsymbol{v}_{H_2} &= \boldsymbol{v}_{CM} + \boldsymbol{u}_{H_2} \quad & \boldsymbol{v}_{e^-} &= \boldsymbol{v}_{CM} + \boldsymbol{u}_{e^-} \\ \boldsymbol{v}'_{H_2} &= \boldsymbol{v}_{CM} + \boldsymbol{u}'_{H_2} \quad & \boldsymbol{v}'_{e^-} &= \boldsymbol{v}_{CM} + \boldsymbol{u}'_{e^-}, \end{aligned} \quad (2)$$

where $\boldsymbol{u}_{H_2}$ and $\boldsymbol{u}_{e^-}$ represent the CM velocities and the primed variables represent the final velocities. These relations can be easily visualized in the Newton diagram from Figure 3. Replacing equation (1) into (2) and using the relative velocity

$$\boldsymbol{g} = \boldsymbol{v}_{H_2} - \boldsymbol{v}_{e^-}, \quad (3)$$

we find

$$\boldsymbol{u}_{H_2} = \frac{m_{e^-}}{m_{H_2} + m_{e^-}}\boldsymbol{g}, \qquad \boldsymbol{u}_{e^-} = -\frac{m_{H_2}}{m_{H_2} + m_{e^-}}\boldsymbol{g}. \quad (4)$$

We have equivalent results for the final velocities $\boldsymbol{u}'_{H_2}$ and $\boldsymbol{u}'_{e^-}$ as a function of the final relative velocity $\boldsymbol{g}' = \boldsymbol{v}'_{H_2} - \boldsymbol{v}'_{e^-}$.

Considering the energy conservation in the collision process, we can write

$$\frac{1}{2}\mu g^2 = \frac{1}{2}\mu g'^2 + \Delta E \quad (5)$$

with the reduced mass $\mu = m_{H_2}m_{e^-}/(m_{H_2} + m_{e^-})$ and $\Delta E$ representing the electron kinetic energy transfered as potential energy to the molecule, i.e., the difference between the excited state energy in the Franck-Condon region and the zero point energy which corresponds to the vibrationless level of the ground electronic state, as shown in Figure 1. Using equation (5), the modulus of the final CM molecular velocity yields:

$$u'_{H_2} = \frac{m_{e^-}}{m_{H_2} + m_{e^-}}g' = \frac{m_{e^-}}{m_{H_2}+m_{e^-}}\sqrt{\frac{2\,(E_{available} - \Delta E)}{\mu}} \quad (6)$$

where $E_{available} = 1/2\ \mu g^2$.

The possible final CM molecular velocity vectors describe the surface of a sphere with radius $u'_{H_2}$ centred at the terminal point of the CM velocity vector $\boldsymbol{v}_{CM}$. The recoil of the molecule is defined by the direction of $\boldsymbol{u}'_{H_2}$, given by the angle $\theta_c$ between $\boldsymbol{u}_{H_2}$ and $\boldsymbol{u}'_{H_2}$ and the azimuthal angle $\phi_c$ referenced to $\boldsymbol{u}_{H_2}$. In our case of an inelastic collision, $u'_{H_2} < u_{H_2}$, as can be seen in Figure 3. Using the possible values for $\Delta E$, i.e., the singly excited vibrational energy levels, which are given in the literature, the recoil of the $H_2$ molecule, $\boldsymbol{v}'_{H_2}$, can be directly computed using vectorial algebra for definite angles $\theta_c$ and $\phi_c$.

In the second step, we consider the isotropic dissociation of $H_2$ molecule in the molecular frame. The centre of mass velocity of this system is $\boldsymbol{v}'_{H_2}$, which direction is defined by the recoil of the $H_2$ molecule. The atoms pair final velocities have the same modulus and opposite directions with respect to the molecule's centre of mass. In the Newton diagram of Figure 4 we show only a $H(2^2S_{1/2})$

atom, as the other atom of the pair, the $H(1^2S_{1/2})$, is not measured. The relationship between the lab and CM velocity vectors $\boldsymbol{v}'_H$ and $\boldsymbol{u}'_H$ is:

$$\boldsymbol{v}'_H = \boldsymbol{v}'_{H_2} + \boldsymbol{u}'_H. \quad (7)$$

The modulus of $\boldsymbol{u}'_H$ is calculated from the theoretical kinetic energy of the $H(2^2S_{1/2})$ in the CM, $E_H$, given by

$$E_H = \frac{\Delta E - D}{2}, \quad (8)$$

where $D$ is 14.68 eV [13] and represents the dissociation energy of the singly excited states, i.e., the energy difference between the asymptotic limit of the excited molecular level and the vibrationless ground electronic state, as shown in Figure 1.

Assuming that the dissociation is isotropic, the possible vectors $\boldsymbol{u}'_H$ describe the surface of a sphere with radius $u'_H$ centred at the end of $\boldsymbol{v}'_{H_2}$ and defined in the molecular CM frame by the angles $\theta_d$ and $\phi_d$. The direction of $\boldsymbol{v}'_H$ in the lab frame is defined by the detector's position; it involves different possible combinations of the molecular recoil and the dissociation angles.

## 4 Analysis of TOF spectra and the origin of the slow $H(2^2S_{1/2})$ atoms

We have varied the electron energy in a range between 9 eV and 200 eV, which encompasses both the threshold for the production of slow and fast $H(2^2S_{1/2})$ atoms. The slow atoms have been detected for all electron energy range, but the fast peak has appeared around 36 eV, as expected. The time-of-flight spectrum for three electron energies are presented in Figure 5. In our following analysis we have used the 120 eV spectra, that corresponds to a typical energy where the relative intensities of the peaks does not vary. In Figure 5 we also show the energy spectra in the molecular CM frame. The transformation from TOF to $E_H$ is discussed in reference [9]. The counting rate is calculated using that

$$N(TOF)dTOF = N(E)dE. \quad (9)$$

The good resolution obtained was due in part to the use of a supersonic jet that produces a beam of $H_2$ molecules with cold internal degrees of freedom. For a thermal jet or gas cell, the kinematical effects explained hereafter would not be visible because the thermal movement of the molecules broadens the velocity distribution [14]. In our case, with Mach number of the order of 10 and with low internal temperature as mentioned before, the initial velocity vector and the levels involved ($v = 0$; $J = 0, 1$) were well defined. The good resolution was also a result of our experimental constraints, as the well defined collision region and the small solid angle of detection.

Among the singly excited states, we are interested in those that produce the pair $H(1^2S_{1/2})+H(2^2S_{1/2})$. As discussed in 1972 by Misakian and Zorn [15] and by Sharp in 1971 [16], in this energy range, between 15−20 eV in the Franck-Condon region, only the $E, F^1\Sigma_g^+$, $a^3\Sigma_g^+$,

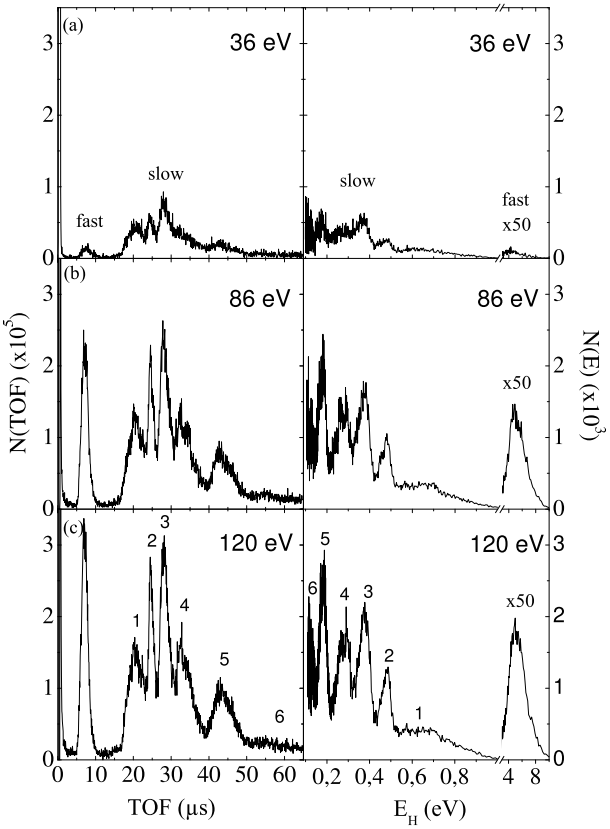


**Fig. 5.** $H(2^2S_{1/2})$ time-of-flight and energy spectra measured after the dissociation of $H_2$ molecules by electrons with 36 eV, 86 eV and 120 eV. The time resolution is limited by the channel width of 128 ns. The graphs (a) show the fast peak near its threshold and in (c) we enumerate the experimental slow peaks referred hereafter.

$B'^1\Sigma_u^+$ and $e^3\Sigma_u^+$ states lead directly to the $H(1^2S_{1/2})$ + $H(2^2S_{1/2})$ dissociation limit. However, they showed that these states cannot be the main source of slow $H(2^2S_{1/2})$.

On the other hand, the states $B'^1\Sigma_u^+$ and $e^3\Sigma_u^+$ are known to mix with the $D^1\Pi_u$ and $d^3\Pi_u$ states. So the slow $H(2^2S_{1/2})$ atoms probably come from the predissociation of these vibrationally excited levels. According to the references cited above, the $d^3\Pi_u$ is more important near the threshold, while for higher excitation energies the most important contribution is from the $D^1\Pi_u$. The structure expected in the spectra was first observed by Mentall and Gentieu [17] in a photodissociation experiment. But, in this case of one photon excitation, the state $d^3\Pi_u$ is forbidden and the peaks were compared with the $D^1\Pi_u$.

Furthermore, it was shown that the $B'^1\Sigma_u^+$ mixes with the $B''^1\Sigma_u^+$ [15,18] and with the $D'^1\Pi_u$ [15,19], which were recently recalculated by Glass-Maujean et al. [20,21]. Their work shows that $B''^1\Sigma_u^+$ is in fact the double well state $B''\overline{B}^1\Sigma_u^+$. According to these authors these states predissociate into $H(1^2S_{1/2})+H(n = 2)$. For the $D'^1\Pi_u$ the contribution comes from the vibrational levels up to $v = 8$ and for the $B''\overline{B}^1\Sigma_u^+$ the coupling occurs at

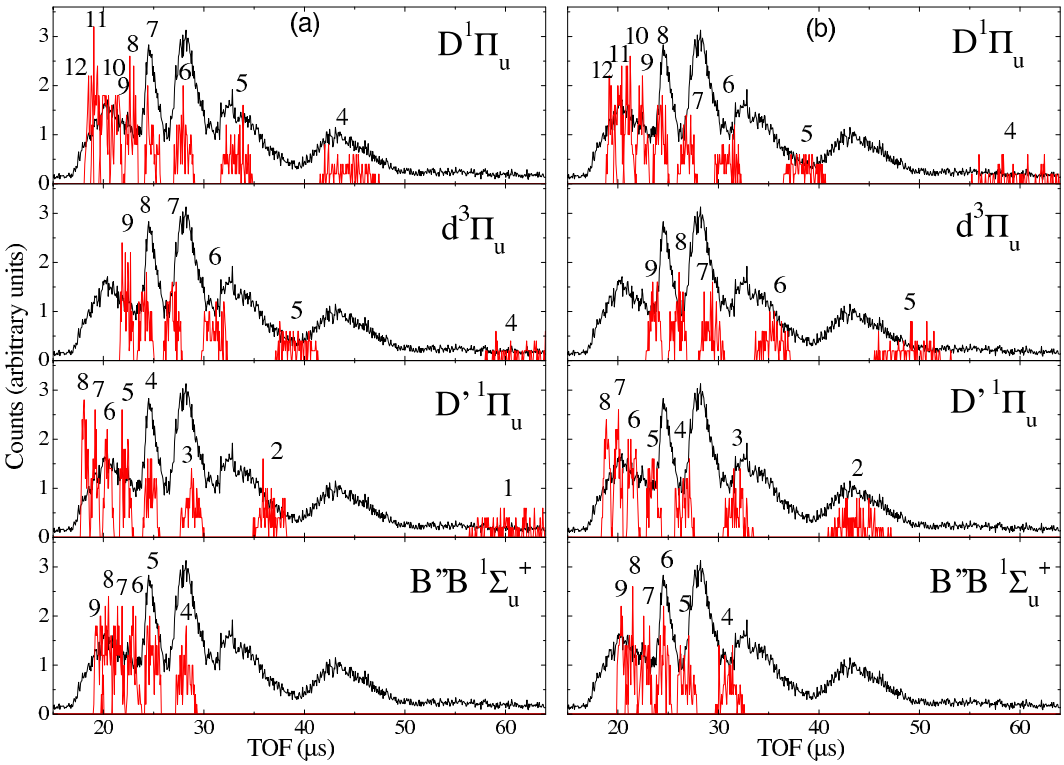


**Fig. 6.** (Color online) Simulated TOF spectra (red line) performed for excitation with 120 eV electrons to the vibrational levels (enumerated in the graphs) of the states $D^1\Pi_u$, $d^3\Pi_u$, $D'^1\Pi_u$ and $B''\overline{B}^1\Sigma_u^+$. (a) Simulation for small $H_2$ recoil angles ($\theta_c$ from 0° to 10°). (b) Simulation for large $H_2$ recoil angles ($\theta_c$ from 170° to 180°). The experimental spectra are shown for comparison.

small internuclear distances, where only the internal well is important.

To assign the vibrational energy levels involved in the predissociation process and to estimate the outcome of the kinematical effects in our spectra, we have simulated by a Monte Carlo method the time-of-flight distribution of the fragments that could arrive at the detection region. We have used $\Delta E$ values given in the literature for the following states $D^1\Pi_u$ [13], $d^3\Pi_u$ [16], $D'^1\Pi_u$ [16,20] and for the inner well of $B''\overline{B}^1\Sigma_u^+$ [21]. Considering that the dissociation represented in Figure 4 is isotropic, we have randomly varied the angles $\theta_d$ from 0° to 180° and $\phi_d$ from 0° to 360°. As we did not have information about the electron impact parameter, we have done a systematic study of the possible recoils of the molecule and compared the simulated spectra with the experimental one.

The angle $\theta_c$, shown in Figure 3, and the azimuthal angle $\phi_c$ define the recoil of the molecule. When all possible angles were taken into account in the same Monte Carlo simulation, the structure of the experimental spectra was not reproduced. There was superposition of the peaks, forming only one broad peak without any structure. Accordingly, we concluded that the possible molecular recoils are not homogeneously distributed.

The peak widths were well reproduced with slices of 10° for $\theta_c$ with $\phi_c$ varying from 0° to 360°. The best agreement with the experimental peaks position was found for small recoil angles, i.e., large impact parameter. We have varied $\theta_c$ from 0° to 10° and obtained the spectrum shown in Figure 6a. For comparison, the spectrum obtained for large recoil angles, with $\theta_c$ varying from 170° to 180°, is shown in Figure 6b. These simulations suggest that small momentum transfers around the minimum recoil are mainly responsible for the measured peaks. Their amplitudes are arbitrary because we do not have information about the weight of each vibrational level in the excitation process. In fact, we expect to extract this information from our results. We have used $10^6$ particles excited to each vibrational energy level.

In the following discussion we refer to the peak numbers shown in Figure 5c.

According to the results of Misakian and Zorn [15], the slowest atoms peak originates from the predissociation of the $d^3\Pi_u$ state. This is in agreement with our simulation from Figure 6a, in which the 4th vibrational level of the $d^3\Pi_u$ state produces the broad and slowest peak. Also according to these authors, all other peaks are formed by the predissociation of the $D^1\Pi_u$ state. This is in agreement with our simulation corresponding to the vibrational levels from $v = 4$ to $v = 12$ of the $D^1\Pi_u$ state. In addition, we observed that the first peak seems to be produced by the overall contribution from $v = 8$ to $v = 12$ levels that are very close, almost in the continuum region.

Figure 6b shows that, for collisions with large recoil angles, the simulated peaks corresponding to the predissociation of $d^3\Pi_u$ state do not agree with the experimental spectra. For the $D^1\Pi_u$ state, the simulation suggests that the $v = 5$ to $v = 8$ levels do not contribute, but we have

found a good agreement in the region of the last experimental peak (from $v = 4$), which is not in accordance with Misakian and Zorn. The $v = 9$ to $v = 12$ levels are very close, almost in the continuum, and in the region of the first peak.

Further, we have also considered in our simulations contributions from $D'^1\Pi_u$ and $B''\overline{B}^1\Sigma_u^+$ states. We found reasonable agreement with the experimental spectra for small recoil angles (Fig. 6a), except for the $v = 2$ level of $D'^1\Pi_u$ state. However, for large recoil angles (Fig. 6b) only the $v = 2$ level of the $D'^1\Pi_u$ state, the $v = 6$ of the $B''\overline{B}^1\Sigma_u^+$ and the levels close to the continuum seems to contribute. But it is not reasonable to assure that an isolated vibrational level of each state predissocites. We conclude that if these states contribute to the $H(2^2S_{1/2})$ spectra, collisions with small recoil angles are also favorable.

The experimental peaks exhibit a broadening due to contributions of different possible recoil angles of the molecule. One can notice that this broadening increases with the time of flight of the atom. As the molecule was excited into bound vibrational levels with a well defined energy, $\Delta E$, this indicates that the width of the slow $H(2^2S_{1/2})$ peaks is essentially determined by the collision kinematics. In all simulations, for a fixed excitation energy, while the slow peaks were reasonably well reproduced, the fast one was essentially a single line in our time scale, meaning that its width was essentially given by the transition from the ground state of $H_2$ to the repulsive doubly excited states. The duration of the electron pulse (1 $\mu$s) also generates a small broadening of the peak.

In order to reproduce the area of each peak and to obtain a quantitative agreement with the experimental spectra, it is necessary to have good estimates of the cross sections for excitation and predissociation of all individual energy levels that we have considered in our simulations. However, slow electron collisions cross sections even for the total destruction cross section of the simplest molecules with very limited range of energies and choice of targets are rarely given in the literature. Recent publications report experiments with very slow electrons (1500−15 000 K) for plasma applications [22] and describe the difficulties in obtaining these values experimentally [23].

As all peaks were simulated in the same conditions, the ratio ($R_k$) between the experimental ($e$) and the simulated ($s_k$) counting rates is proportional to the cross section of the corresponding $k$ energy level. Thus, assuming that the processes occur at small recoil angles (condition of Fig. 6a), we have minimized the difference between each experimental peak and its probable simulated contributions in the parameter $R_k$ by using the least square method, i.e.,

$$\text{Min}\sum_i \frac{(\sum_k R_k \cdot s_{ki} - e_i)^2}{e_i^2}, \tag{10}$$

where $i$ sweeps the time-of-flight interval of each experimental peak. Considering the fluctuations of the experimental and of the simulated spectra, we obtained a mean error of 12% for the $R_k$ parameters.

First, according to Misakian and Zorn [15], we have considered that the spectra is formed only by the $v = 4$ level of $d^3\Pi_u$ state for the last peak, while all other peaks are produced by the predissociation of the $D^1\Pi_u$. In this way, the $k$ energy levels that contribute to each slow experimental peak, referred in Figure 5c, are:

1st: $v = 8, v = 9, v = 10, v = 11, v = 12$ of $D^1\Pi_u$;
2nd: $v = 7$ of $D^1\Pi_u$;
3rd: $v = 6$ of $D^1\Pi_u$;
4th: $v = 5$ of $D^1\Pi_u$;
5th: $v = 4$ of $D^1\Pi_u$;
6th: $v = 4$ of $d^3\Pi_u$.

And this leads to the ratios:

| energy level ($k$) | $R_k$ |
|---|---|
| $d^3\Pi_u$, $v = 4$ | 1.1 |
| $D^1\Pi_u$, $v = 4$ | 3.9 |
| $D^1\Pi_u$, $v = 5$ | 3.7 |
| $D^1\Pi_u$, $v = 6$ | 5.3 |
| $D^1\Pi_u$, $v = 7$ | 4.5 |
| $D^1\Pi_u$, $v = 8$ | 1.5 |
| $D^1\Pi_u$, $v = 9$ | 1.8 |
| $D^1\Pi_u$, $v = 10$ | 2.0 |
| $D^1\Pi_u$, $v = 11$ | 1.0 |
| $D^1\Pi_u$, $v = 12$ | 1.1 |

Adding the $D'^1\Pi_u$ and $B''\overline{B}^1\Sigma_u^+$ contributions makes it difficult to deduce any precise information in the region of the first experimental peak, where many levels near the continuum seems to contribute. Therefore, we have considered only the remaining ones. In order to get the total $\sum_k R_k \cdot s_k$ signal for each peak (2nd to 6th) we summed up the contributions of the relevant following levels:

2nd: $v = 7$ of $D^1\Pi_u, v = 4$ of $D'^1\Pi_u, v = 5$ of $B''\overline{B}^1\Sigma_u^+$;
3rd: $v = 6$ of $D^1\Pi_u, v = 3$ of $D'^1\Pi_u, v = 4$ of $B''\overline{B}^1\Sigma_u^+$;
4th: $v = 5$ of $D^1\Pi_u, v = 2$ of $D'^1\Pi_u$;
5th: $v = 4$ of $D^1\Pi_u$;
6th: $v = 4$ of $d^3\Pi_u, v = 1$ of $D'^1\Pi_u$.

In this way, we found the following ratios for each state:

| energy level ($k$) | $R_k$ |
|---|---|
| $d^3\Pi_u$, $v = 4$ | 0.6 |
| $D^1\Pi_u$, $v = 4$ | 3.9 |
| $D^1\Pi_u$, $v = 5$ | 3.7 |
| $D^1\Pi_u$, $v = 6$ | 2.0 |
| $D^1\Pi_u$, $v = 7$ | 0.1 |
| $D'^1\Pi_u$, $v = 1$ | 0.8 |
| $D'^1\Pi_u$, $v = 2$ | 2.1 |
| $D'^1\Pi_u$, $v = 3$ | 4.2 |
| $D'^1\Pi_u$, $v = 4$ | 2.5 |
| $B''\overline{B}^1\Sigma_u^+$, $v = 4$ | 1.7 |
| $B''\overline{B}^1\Sigma_u^+$, $v = 5$ | 1.9 |

It should be noted that the references [20,21] do not differentiate if the states $B''^1\Sigma_u^+$ and $D'^1\Pi_u$ predissociate into $H(2^2S_{1/2})$ or $H(2^2P_{1/2})$, then we cannot conclude which of the two cases above is more suitable. However, there is an agreement concerning the 5th peak, which is formed only by the $v = 4$ of $D^1\Pi_u$ with $R_k = 3.9$. In addition, the 4th peak has $v = 5$ of $D^1\Pi_u$ with $R_k = 3.7$ in both cases. As the states $v = 5$ of $D^1\Pi_u$ and $v = 2$ of $D'^1\Pi_u$ do not overlap, the second one was added to the fit without changing the weight of the $v = 5$ of $D^1\Pi_u$.

It is worth to mention that a similar analysis was accomplished by Ryan et al. [19] despite their low spectrum resolution. They used empirical gaussians in energy and considered all peaks with the same width, in opposition to our conclusion that the width of the peaks are a function of the energy (or TOF).

## 5 Conclusions

The main characteristics of this experiment are the low ro-vibrational temperature of $H_2$ molecules, the long flight path and the small well defined collision and electric field regions. These characteristics lead us to get precise velocity measurements and, consequently, a good spectra resolution.

If dissociation by laser excitation can achieve better precision and resolution, electron collisions can excite levels that are forbidden by one photon absorption. Moreover, the dissociation by electron impact enabled us to evidence aspects that are not present in the laser excitation experiments: we have carefully analysed the collisional constraints, as the recoil angle and its influence on the peak width.

Using Newton diagrams we have simulated the TOF peaks generated by the excitation and subsequent dissociation of all relevant singly excited states. Comparing the simulation with the experimental results we have inferred that collisions at large impact parameter are the most favorable for this $H_2$-electron collision at 120 eV. The simulation has also allowed us to assign the vibrational levels of the singly excited states of $H_2$ molecule that lead to the dissociation channel producing slow $H(2^2S_{1/2})$ atoms. The analysis of the kinematical effects on the peak widths has showed that the peak broads with the inverse of the velocity of the $H(2^2S_{1/2})$ atoms.

Comparing the simulated and experimental peak amplitudes, we have estimated the relative excitation probabilities of each vibrational level predissociating into the pair $H(2^2S_{1/2}) + H(1^2S_{1/2})$.

This work is supported by FAPERJ, CNPq and the Scientific Cooperation Agreement CAPES/COFECUB between France and Brazil. R.C. gratefully acknowledge CNRS for her postdoctoral fellowship for the project "Twin atoms" and F. Zappa is grateful to FAPEMIG for financial support.

## References

1. X. Liu, P.V. Johnson, C.P. Malone, J.A. Young, D.E. Shemansky, I. Kanik, J. Phys. B: At. Mol. Opt. Phys. **42**, 185203 (2009)
2. D.E. Shemansky, X. Liu, H. Melin, Planet. Space Sci. **57**, 1659 (2009)
3. J.L. Terry, J. Vac. Sci. Technol. A **1**, 831 (1983)
4. Y.V. Vanne, A. Saenz, A. Dalgarno, R.C. Forrey, P. Froelich, S. Jonsell, Phys. Rev. A **73**, 062706 (2006)
5. M. Glass-Maujean, Ch. Jungen, H. Schmoranzer, A. Knie, I. Haar, R. Hentges, W. Kielich, K. Jänkälä, A. Ehresmann, Phys. Rev. Lett. **104**, 183002 (2010)
6. R.C. Forrey, R. Côté, A. Dalgarno, S. Jonsell, A. Saenz, P. Froelich, Phys. Rev. Lett. **85**, 4245 (2000)
7. D. Landhuis, L. Matos, S.C. Moss, J.K. Steinberger, K. Vant, L. Willmann, T.J. Greitak, D. Kleppner, Phys. Rev. A **67**, 022718 (2003)
8. M. Leventhal, R.T. Robiscoe, K.R. Lea, Phys. Rev. **158**, 49 (1967)
9. A. Medina, G. Rahmat, C.R. de Carvalho, G. Jalbert, F. Zappa, R.F. Nascimento, R. Cireasa, N. Vanhaecke, I.F. Schneider, N.V. de Castro Faria, J. Robert, J. Phys. B: At. Mol. Opt. Phys. **44**, 215203 (2011)
10. R. Campargue, J. Phys. Chem. **88**, 4466 (1984)
11. V. Cavero-Manchado, *La collision réactive* $Li(3s) + H_2 \rightarrow LiH + H$. *Transfert de structure fine entre isotopes du lithium dans un jet unique*, Ph.D. thesis, Université Paris-Sud, Orsay, 1997
12. R. Campargue, A. Lebehot, J.C. Lemonnier, D. Marette *Rarefied Gas Dynamics*, edited by S.S. Fisher (AIAA, New York, 1981), p. 823
13. K. Dressler, L. Wolniewicz, J. Chem. Phys. **85**, 2821 (1986)
14. G. Vassilev, F. Perales, Ch. Miniatura, J. Robert, J. Reinhardt, F. Vecchiocattivi, J. Baudon, Z. Phys. D **17**, 101 (1990)
15. M. Misakian, J.C. Zorn, Phys. Rev. A **6**, 2180 (1972)
16. T.E. Sharp, At. Data **2**, 119 (1971)
17. J.E. Mentall, E.P. Gentieu, J. Chem. Phys. **52**, 5641 (1970)
18. F.J. Comes, U. Wenning, Z. Naturforsch. A **25**, 237 (1970)
19. S.R. Ryan, J.J. Spezeski, O.F. Kalman, W.E. Lamb Jr., L.C. McIntyre Jr., W.H. Wing, Phys. Rev. A **19**, 2192 (1979)
20. M. Glass-Maujean, S. Klumpp, L. Werner, A. Ehresmann, H. Schmoranzer, J. Chem. Phys. **128**, 094312 (2008)
21. M. Glass-Maujean, S. Klumpp, L. Werner, A. Ehresmann, H. Schmoranzer, J. Chem. Phys. **126**, 144303 (2007)
22. R. Riahi, Ph. Teulet, Z. Ben Lakhdar, A. Gleizes, Eur. Phys. J. D **40**, 223 (2006)
23. J.S. Yoon, M.Y. Song, J.M. Han, S.H. Hwang, W.S. Chang, B. Lee, Y. Itikawa, J. Phys. Chem. Ref. Data **37**, 913 (2008)